

Fermi-surface study of $\text{Ba}_{1-x}\text{K}_x\text{BiO}_3$

S. Sahrakorpi

Institute of Physics, Tampere University of Technology, 33101 Tampere, Finland

B. Barbiellini and R. S. Markiewicz

Department of Physics, Northeastern University, Boston, Massachusetts 02115

S. Kaprzyk

*Department of Physics, Northeastern University, Boston, Massachusetts 02115
and Academy of Mining and Metallurgy AGH, 30059 Kraków, Poland*

M. Lindroos

*Institute of Physics, Tampere University of Technology, 33101 Tampere, Finland
and Department of Physics, Northeastern University, Boston, Massachusetts 02115*

A. Bansil

Department of Physics, Northeastern University, Boston, Massachusetts 02115

(Received 18 August 1999)

We present all-electron computations of the three-dimensional (3D) Fermi surfaces (FS's) in $\text{Ba}_{1-x}\text{K}_x\text{BiO}_3$ for a number of different compositions based on the self-consistent Korringa-Kohn-Rostoker coherent-potential-approximation approach for incorporating the effects of Ba/K substitution. By assuming a simple cubic structure throughout the composition range, the evolution of the nesting and other features of the FS of the underlying pristine phase is correlated with the onset of various structural transitions with K doping. A parametrized scheme for obtaining an accurate 3D map of the FS in $\text{Ba}_{1-x}\text{K}_x\text{BiO}_3$ for an arbitrary doping level is developed. We remark on the puzzling differences between the phase diagrams of $\text{Ba}_{1-x}\text{K}_x\text{BiO}_3$ and $\text{BaPb}_x\text{Bi}_{1-x}\text{O}_3$ by comparing aspects of their electronic structures and those of the end compounds BaBiO_3 , KBiO_3 , and BaPbO_3 . Our theoretically predicted FS's in the cubic phase are relevant for analyzing high-resolution Compton scattering and positron-annihilation experiments sensitive to the electron momentum density, and are thus amenable to substantial experimental verification.

I. INTRODUCTION

The cubic perovskite $\text{Ba}_{1-x}\text{K}_x\text{BiO}_3$,^{1,2} which achieves a maximum transition temperature of 32 K (for $x \approx 0.4$), has been the subject of numerous studies. Despite some similarity to the better known high- T_c cuprates, the system is three dimensional and lacks strong magnetic properties in the normal state. The vibrational breathing mode of the BiO_6 octahedra appears to yield a strong electron-phonon coupling³⁻⁶ which together with dielectric effects may explain the superconducting properties.^{7,8} However, recently observed anomalous temperature dependencies of the critical magnetic fields and vanishing discontinuities in the specific heat and magnetic susceptibility suggest a fourth-order transition to superconductivity.⁹ Therefore, in contrast to the standard BCS picture, thermodynamic properties seem almost unchanged through the transition.

$\text{Ba}_{1-x}\text{K}_x\text{BiO}_3$ also possesses a rich structural phase diagram^{10,11} as a function of K doping. In the range $0 < x < 0.12$, the system assumes a monoclinic structure which can be obtained from the cubic structure via small tilting and breathing distortions of the BiO_6 octahedra; in the undoped compound the tilting angle along (1,1,0) is estimated to be 11.2° and the breathing distortion to be 0.085 \AA . For $0.12 < x < 0.37$, the structure is orthorhombic, admitting tilting

but not breathing distortion. Finally, for $0.37 < x < 0.53$, when the cubic phase is stabilized, the system becomes metallic. Although it is widely believed that the insulating phases for $x < 0.37$ are caused by charge density instabilities associated with the breathing and tilting distortions, it has proven difficult to establish this in terms of first principles computations. Very recent total energy calculations on distorted lattices⁵ indicate that, in contrast to earlier results,⁴ the local-density approximation (LDA) substantially underestimates the size of the breathing distortion and yields a metallic ground state. Perhaps correlation corrections beyond the LDA are necessary in order to explain the insulating phases.

In this article, we report highly accurate, all-electron computations of three-dimensional (3D) Fermi surfaces in $\text{Ba}_{1-x}\text{K}_x\text{BiO}_3$ for a number of different compositions. All calculations pertain to the simple cubic (sc) lattice and are parameter free except for the use of the Korringa-Kohn-Rostoker coherent-potential approximation (KKR-CPA) to treat the effects of Ba/K substitution, and the local density approximation for treating exchange-correlation effects. Our motivation for invoking the sc structure throughout the composition range is that in this way we are in a position to focus on the evolution of nesting and other features of the Fermi surface (FS) in the underlying pristine phase and to delineate how the appearance of such features correlates with the onset

of various structural transitions with K doping. Note that lattice distortions in $\text{Ba}_{1-x}\text{K}_x\text{BiO}_3$ are relatively small, and pseudocubic lattice parameters are easily assigned in all cases.

Our computations show clearly that the highest occupied band in BaBiO_3 , in which the FS resides, remains virtually unchanged in shape upon substituting Ba with K, and that the associated states near the Fermi energy (E_F) continue to possess long lifetimes since they suffer little disorder-induced scattering in the alloy. This circumstance allows us to fit this band in BaBiO_3 in terms of a Fourier-like expansion which accurately describes the highest occupied band in $\text{Ba}_{1-x}\text{K}_x\text{BiO}_3$ for *all compositions* x ; a knowledge of the E_F then yields the corresponding FS. In this way, we provide a useful parametrized form that permits a straightforward determination of the full 3D Fermi surface in cubic $\text{Ba}_{1-x}\text{K}_x\text{BiO}_3$ for any arbitrary K doping level.

Highlights of some of the issues addressed together with an outline of this article are as follows. Section II gives an overview of the methodology and provides associated technical details of the computations. The presentation of results in Sec. III is subdivided into several subsections. Subsection III A discusses changes in topology of the FS with K doping and attempts to correlate these changes with the observed structural transformations in $\text{Ba}_{1-x}\text{K}_x\text{BiO}_3$ invoking Hume-Rothery and Van Hove–Jahn-Teller scenarios. Subsection III B takes up the question of parametrizing the FS, and gives details of the parameters that describe the doping-dependent FS of cubic $\text{Ba}_{1-x}\text{K}_x\text{BiO}_3$. Subsection III C compares aspects of the electronic structures of $\text{Ba}_{1-x}\text{K}_x\text{BiO}_3$ and $\text{BaPb}_x\text{Bi}_{1-x}\text{O}_3$ as well as those of the end compounds BaBiO_3 , KBiO_3 , and BaPbO_3 with an eye toward understanding some puzzling differences between the phase diagrams of $\text{Ba}_{1-x}\text{K}_x\text{BiO}_3$ and $\text{BaPb}_x\text{Bi}_{1-x}\text{O}_3$. Subsection III D discusses how our theoretical FS's for the cubic phase are relevant for analyzing experiments sensitive to the momentum density of the electron gas (positron annihilation, high-resolution Compton scattering), and are thus amenable to substantial experimental verification; a recent angle-resolved photoelectron spectroscopy measurement of doping dependence of the chemical potential in $\text{Ba}_{1-x}\text{K}_x\text{BiO}_3$ is also discussed in order to gain insight into the band renormalization at the Fermi energy. Section IV summarizes our conclusions. Finally, concerning related work, it may be noted that we are not aware of a systematic study of the evolution of the FS of $\text{Ba}_{1-x}\text{K}_x\text{BiO}_3$ with K doping in the literature, although aspects of the problem have been commented upon by various authors.^{5,6,12,13}

II. OVERVIEW OF METHODOLOGY AND COMPUTATIONAL DETAILS

Before proceeding with the computation of the FS for a given K doping x , we first obtained the charge self-consistent KKR-CPA crystal potential in $\text{Ba}_{1-x}\text{K}_x\text{BiO}_3$ assuming random substitution of Ba by K; for details of our KKR-CPA methodology, we refer to Refs. 14–16. The charge as well as the KKR-CPA self-consistency cycles have been carried out to a high degree of convergence in all cases; for example, the final Fermi energies are accurate to about 2 mRy and the total charge within each of the muffin-tin spheres to about

10^{-3} electrons. The total energies were not minimized to determine the lattice constants. The experimental lattice data were used instead, but otherwise the computations are parameter free. The simple cubic lattice constants used for BaBiO_3 and KBiO_3 are 4.3485 Å and 4.2886 Å, respectively.¹¹ For intermediate compositions, lattice constants were obtained via Vegard's law. The muffin-tin radii of Bi and O were taken to be $a/4$, where a denotes the composition-dependent lattice constant. The radius of the Ba or K sphere (recall that within the KKR-CPA scheme the two radii must be equal as these atoms occupy the same site randomly) was chosen by requiring the Ba/K sphere to touch the O sphere, which gives the value $(1/\sqrt{2}-1/4)a$ for the Ba/K radius.¹⁴ The aforementioned choices of the radii provide a good convergence of the crystal potential, and in any event, the results are not sensitive to these details. The calculations employ the Barth-Hedin exchange-correlation functional¹⁷ and are semirelativistic with respect to the valence states, but the core states are treated relativistically. However, the relativistic effects on the valence states are expected to be small. In particular, the band giving rise to the FS is built mainly from the Bi $6s$ and O $2p$ orbitals, which are affected little by the spin-orbit coupling; the effect of Bi $6p$ admixture on the bands is estimated to be on the order of 0.1 eV.¹² The maximum l cutoffs used are $l_{max}=3$ for Ba, K, and Bi sites, and $l_{max}=2$ for O atoms.

Once the self-consistent crystal potential is determined using the preceding procedure, the Fermi surface in a disordered alloy is computed by evaluating the spectral density function $A(\mathbf{p}, E) = -(1/\pi)\text{Im}[G(\mathbf{p}, E)]$, where $G(\mathbf{p}, E)$ is the one-particle ensemble averaged KKR-CPA Green function at a given momentum \mathbf{p} and energy E . The radius of the FS along a given direction $\hat{\mathbf{p}}$ is then defined by the position of the peak in $A(p, E)$ at $E=E_F$; the finite width of the spectral peaks reflects the disorder-induced scattering of states, and would in general yield a FS in an alloy that is smeared or blurred.^{18,19} In the present case of $\text{Ba}_{1-x}\text{K}_x\text{BiO}_3$, however, it turns out that the Bi-O states near the E_F are virtually unaffected by Ba/K substitution and therefore suffer little damping (≈ 1 mRy). For this reason, the KKR-CPA variations in the E_F in $\text{Ba}_{1-x}\text{K}_x\text{BiO}_3$ are also close to the rigid band values based on the BaBiO_3 band structure. In order to obtain the highly accurate 3D maps of the FS discussed below, a uniform net of about 10^5 \mathbf{k} points in the irreducible Brillouin zone has been employed. Finally, we note that the specific parameters used in the density of states and related computations on $\text{BaPb}_x\text{Bi}_{1-x}\text{O}_3$ presented in this work are similar to those detailed above; the lattice constant of BaPbO_3 was 4.2656 Å.²⁰

III. RESULTS AND DISCUSSION

A. Evolution of the Fermi surface with doping; structural transitions

Figures 1–4 present 3D images of the FS in the cubic phase for K concentrations $x=0.67, 0.40, 0.13$, and 0.0, together with three different cross sections in the (001) and (110) planes. With reference to these figures we will discuss how nesting features evolve and correlate with the occurrence of structural transitions in $\text{Ba}_{1-x}\text{K}_x\text{BiO}_3$ with K doping.

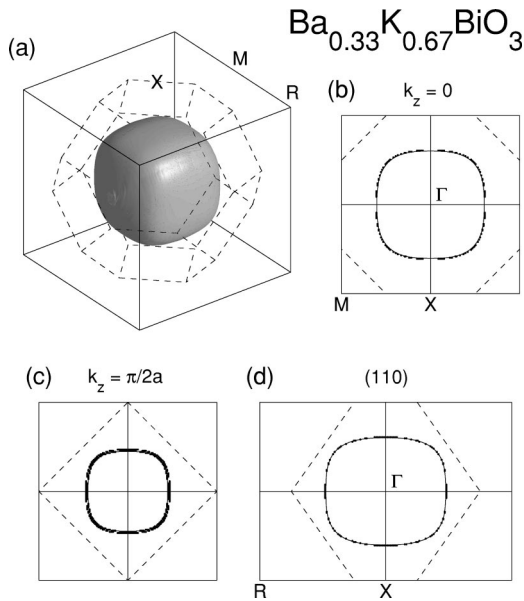


FIG. 1. Fermi surface of cubic $\text{Ba}_{1-x}\text{K}_x\text{BiO}_3$ for $x=0.67$. (a) gives a 3D rendition, while (b) and (c) are two (001) sections at $k_z=0$ and $k_z=\pi/2a$. (d) is a (110) section through the zone center. The boundaries of the simple cubic zone (solid) as well as those of the bcc zone (dashed) are shown. Points in (b)–(d) are the computed KKR-CPA values while the associated solid curves are the fits to the FS based on Eqs. (1) and (2) discussed in the text. The disorder-induced smearing of the FS is very small and is not shown.

The FS for $x=0.67$ is shown in Fig. 1. The composition is at the upper limit of stability ($x\approx 0.6-0.7$) of the cubic phase. The FS is a flattened free-electron-like sphere which appears nearly cubic in shape. This is evident in the 3D rendition of Fig. 1(a) as well as in the squarish appearance of sections of Figs. 1(b) and 1(c). Our computations indicate that the FS becomes even more cubelike for $x>0.67$ (not shown); since the cubic shape is particularly susceptible to

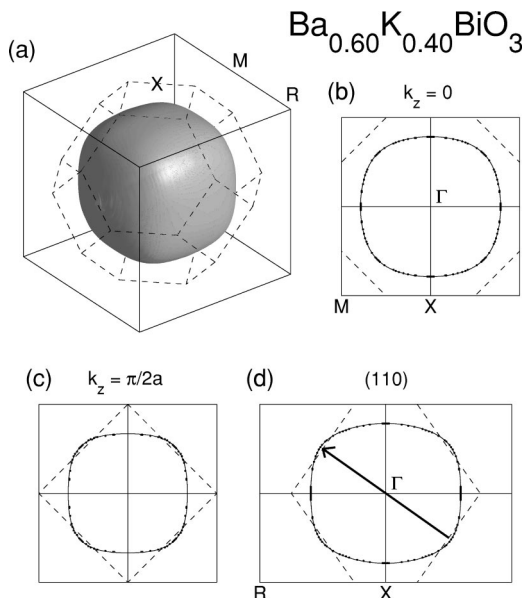


FIG. 2. Same as the caption to Fig. 1 except $x=0.4$. The arrow shows the spanning vector along (111) related to the Hume-Rothery instability to the orthorhombic phase discussed in the text.

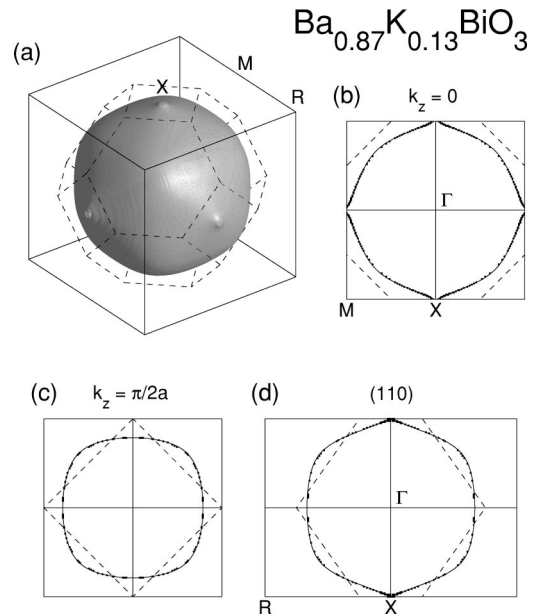


FIG. 3. Same as the caption to Fig. 1 except $x=0.13$. The FS is seen to make contact with the Brillouin zone boundary around the X points.

nesting, one may speculate a connection with the aforementioned phase stability limit. Incidentally, asphericity of the FS introduces momentum dependence in the Eliashberg equation with subtle consequences for superconducting properties.²¹

With decreasing x , the FS grows in size as seen in Fig. 2 for $x=0.40$; this composition has been chosen to lie close to the cubic-orthorhombic phase boundary at $x=0.37$. Since the orthorhombic unit cell is very similar to fcc,¹² the associated Brillouin zone (BZ) is also drawn in Fig. 2. The FS is seen to make contact with the hexagonal face of the bcc zone; this is more clear in the (110) section of Fig. 2(d). These results suggest that the cubic-orthorhombic transition may be

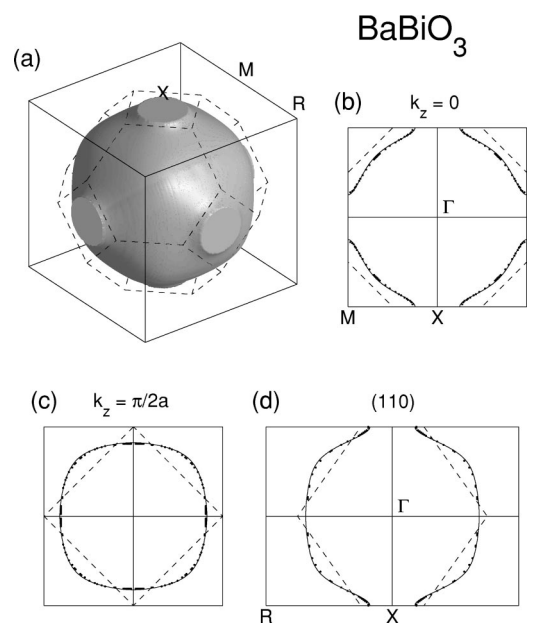


FIG. 4. Same as the caption to Fig. 1 except $x=0$, referring to BaBiO_3 .

viewed as a Hume-Rothery type structural instability²² to some larger unit cell that arises when the FS crosses the BZ of the associated supercell. We find that the FS becomes tangent to the hexagonal face at $x=0.45$. Note that the Hume-Rothery rules require the transition to occur not at the point of first contact with the BZ, but after the FS has grown to slightly overlap the zone boundary.²³ In the present case these arguments would thus predict a transition to a fcc structure at $x \approx 0.4$ where the cubic FS has already broken through the zone boundary. Recall that the orthorhombic structure involves lattice distortions via tilting mode phonons with wave vector $\mathbf{R} = (1,1,1)\pi/a$,^{4,5} which is consistent with Fig. 2(d) where the spanning vector (denoted by the arrow) is indeed seen to be approximately equal to \mathbf{R} .

It is noteworthy that different Hume-Rothery phases presumably involve a succession of free energy minima as a function of composition.²³ If so, there is the possibility that the system will actually go into a mixed phase at the transition, similar to the mixed α plus β phase in brasses.²⁴ In the $\text{Ba}_{1-x}\text{K}_x\text{BiO}_3$ system, an incommensurate modulation has been observed by electron but not neutron diffraction,¹¹ suggestive of a fluctuating or nanoscale phase separation, which is reminiscent of the stripelike phases found in the cuprates and related oxides.

We consider Fig. 3 next for $x=0.13$ where $\text{Ba}_{1-x}\text{K}_x\text{BiO}_3$ undergoes the orthorhombic to monoclinic transition. Compared to $x=0.40$ (Fig. 2), the FS has become more rounded. The most striking feature however is that the FS has grown to just begin making contact with the zone boundary at the X point. In fact, the band structure of cubic BaBiO_3 (see Sec. III C below) contains a saddle point at X which lies approximately 0.1 eV below the Fermi energy. The associated Van Hove singularity (VHS) in the density of states crosses the Fermi level around $x \approx 0.13$ and gives rise to the change in the FS topology seen in Fig. 3. Computations of Ref. 4 indicate that the electron-phonon coupling parameter λ can increase sharply as x decreases below 0.13 causing the breathing mode phonon to become unstable.

It is interesting to ask the question: Since the orthorhombic and monoclinic distortions possess nearly the same fcc BZ, what is the driving force behind the transformation at $x=0.13$? The FS of Fig. 3 suggests an interpretation in terms of a Van Hove–Jahn-Teller scenario.^{25,26} When the VHS intersects the Fermi energy, there are three independent VHS's whose degeneracy cannot be lifted in the orthorhombic phase. Since each VHS involves a substantial density of states, the system can gain energy via a Jahn-Teller distortion to a lower-symmetry phase (such as monoclinic) which lifts the degeneracy between the VHS's.

Figure 4 shows the FS of cubic BaBiO_3 for completeness. The FS is a distorted sphere with large necks at X. No significant changes in the topology of the FS take place over the composition range $0 < x < 0.13$.

B. A parametrized form for the doping-dependent Fermi surface

We fit first the Bi $6s-O2p$ band $E(k_x, k_y, k_z)$ in BaBiO_3 (see Fig. 5), which gives rise to the FS, in terms of the following Fourier-like expansion:

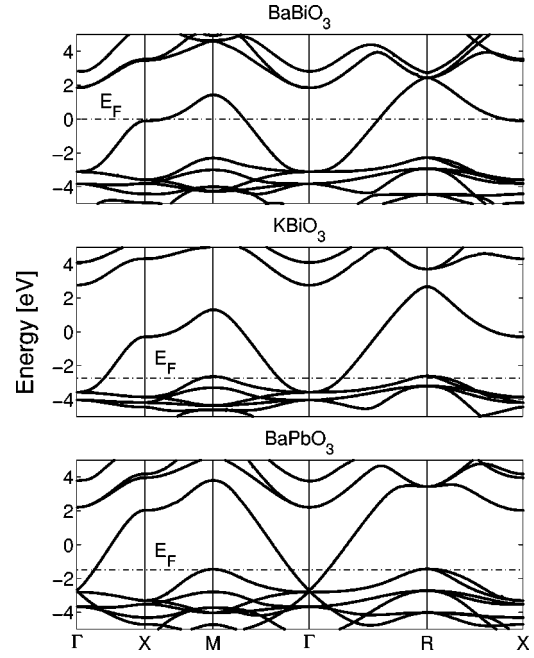


FIG. 5. Band structures of BaBiO_3 , KBiO_3 , and BaPbO_3 along high-symmetry directions are compared in the vicinity of the Fermi energy E_F (dot-dashed horizontal lines).

$$\begin{aligned}
 E(k_x, k_y, k_z) = & E_0 + t_1(X + Y + Z) + t_2(XY + XZ + YZ) \\
 & + t_3XYZ + t_4(X_2 + Y_2 + Z_2) \\
 & + t_5(XY_2 + XZ_2 + YZ_2 + X_2Y + X_2Z + Y_2Z) \\
 & + t_6(X_2Y_2 + X_2Z_2 + Y_2Z_2), \quad (1)
 \end{aligned}$$

where $X = \cos(k_x a)$, $Y = \cos(k_y a)$, $Z = \cos(k_z a)$, $X_2 = \cos(2k_x a)$, $Y_2 = \cos(2k_y a)$, $Z_2 = \cos(2k_z a)$; a is the lattice constant and E_0 is the average band energy. The k dependence on the right side of Eq. (1) possesses the form of a tight-binding band and in this sense t_n may be viewed as the n th nearest neighbor ‘‘hopping integral.’’ The values of various parameters which fit the computed 3D band are (in eV) $E_0 = -0.288$ (with respect to the Fermi level of BaBiO_3), $t_1 = -0.6191$, $t_2 = -0.4313$, $t_3 = 0.0816$, $t_4 = 0.1034$, $t_5 = 0.1361$, and $t_6 = -0.0449$. Higher-order terms in the expansion are found to be negligibly small. The fit is valid throughout the composition range in $\text{Ba}_{1-x}\text{K}_x\text{BiO}_3$ since, as already noted, the Bi $6s-O2p$ band remains essentially unchanged in shape near the E_F with K/Ba substitution. The fact that the terms with t_3-t_6 are significant in obtaining an accurate fit indicates that the associated interaction parameters possess a fairly long range. Incidentally, supercell simulations indicate that electronic states near the Fermi level are not sensitive to short-range ordering effects.¹³

The constant-energy surface can now be obtained for any given value of the energy by solving Eq. (1); in order to obtain the FS at a given doping, we need only specify the corresponding value of the E_F . For this purpose, we have parametrized the KKR-CPA values of $E_F(x)$ in $\text{Ba}_{1-x}\text{K}_x\text{BiO}_3$ as a second-order polynomial:

$$E_F(x) = a_1 x^2 + a_2 x, \quad (2)$$

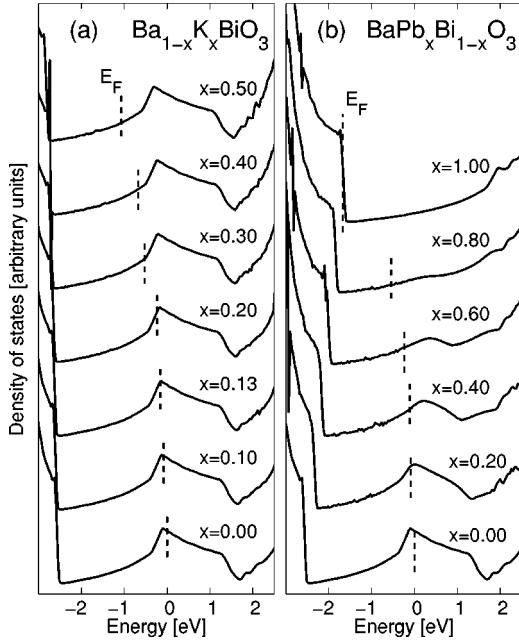


FIG. 6. Self-consistent KKR-CPA densities of states in the vicinity of the Fermi energy in (a) $\text{Ba}_{1-x}\text{K}_x\text{BiO}_3$ and (b) $\text{BaPb}_x\text{Bi}_{1-x}\text{O}_3$ over the composition ranges x indicated. Vertical dashed lines give Fermi energies.

where $E_F=0$ for $x=0$, $a_1=-2.078$ eV, and $a_2=-0.6612$ eV. The solid lines in the sections of Figs. 1–4 show that Eqs. (1) and (2) provide an excellent fit to the 3D Fermi surface in $\text{Ba}_{1-x}\text{K}_x\text{BiO}_3$ over the entire composition range. Notably, the positive sign of the ratio $\tau=t_2/t_1$ reflects a concave down curving of the FS in the basal plane (see Figs. 1–4); in contrast, some cuprates possess FS’s curving concave up.²⁷ For the special case where only the nearest neighbor hopping term t_1 is considered in Eq. (1), the FS will be perfectly nested at half filling, and hence unstable with respect to infinitesimal perturbations; the presence of interactions with neighbors farther out smears this singularity, although some softness in the system remains as already discussed above.

C. $\text{Ba}_{1-x}\text{K}_x\text{BiO}_3$ vs $\text{BaPb}_x\text{Bi}_{1-x}\text{O}_3$

Despite substantial similarities, the phase diagrams of $\text{Ba}_{1-x}\text{K}_x\text{BiO}_3$ and $\text{BaPb}_x\text{Bi}_{1-x}\text{O}_3$ display significant differences. The monoclinic to orthorhombic transition occurs at roughly the same doping level in both systems, but the orthorhombic phase in $\text{BaPb}_x\text{Bi}_{1-x}\text{O}_3$ persists up to 0.6 holes per band, and unlike $\text{Ba}_{1-x}\text{K}_x\text{BiO}_3$, it does not undergo the transition to the cubic phase. Since the FS’s of $\text{Ba}_{1-x}\text{K}_x\text{BiO}_3$ and $\text{BaPb}_x\text{Bi}_{1-x}\text{O}_3$ may be expected to be roughly similar (in view of similarities of their electronic structures), on the face of it, the explanations of Sec. III A above for $\text{Ba}_{1-x}\text{K}_x\text{BiO}_3$ would appear to be applicable also to $\text{BaPb}_x\text{Bi}_{1-x}\text{O}_3$. Some insight into the puzzling behavior of $\text{BaPb}_x\text{Bi}_{1-x}\text{O}_3$ may be obtained by comparing the band structures near the Fermi energy of the end compounds BaBiO_3 , KBiO_3 , and BaPbO_3 shown in Fig. 5, and the associated composition-dependent densities of states in $\text{Ba}_{1-x}\text{K}_x\text{BiO}_3$ and $\text{BaPb}_x\text{Bi}_{1-x}\text{O}_3$ (Fig. 6).

The important point to note is that the band passing through the Fermi energy in BaBiO_3 as well as KBiO_3 is a hybridized Bi-O band which is affected little when Ba is substituted by K in $\text{Ba}_{1-x}\text{K}_x\text{BiO}_3$; the associated density of states in Fig. 6(a) displays two distinct features near zero and 1.4 eV (in BaBiO_3) which are weakly doping dependent. In sharp contrast, in $\text{BaPb}_x\text{Bi}_{1-x}\text{O}_3$ the valence band changes from Bi-O to Pb-O, and the VHS’s in the end compounds BaBiO_3 and BaPbO_3 lie around -0.1 eV and 2.0 eV, respectively, Fig. 6(b). [Structure from higher bands is evident above 2 eV in Fig. 6(b).] As a result, the density of states of $\text{BaPb}_x\text{Bi}_{1-x}\text{O}_3$ alloys is characterized by a ‘‘split-band’’ behavior:^{18,19} when Bi is substituted by Pb, the VHS around -0.1 eV arising from the Bi-O band gradually loses spectral weight which gets transferred to the VHS around 2.0 eV of the PbO band. Consequently, states near the Fermi level will suffer substantial disorder-induced scattering.¹⁴ The FS in $\text{BaPb}_x\text{Bi}_{1-x}\text{O}_3$ will then be quite smeared, rendering suspect the arguments of Sec. III A which assume a sharply defined FS.

D. Comparison with experiments

We note first that the theoretically predicted FS for the cubic phase at $x=0.4$ (Fig. 1) is in good accord with the experimental FS deduced by Mosley *et al.*²⁸ from positron-annihilation measurements. As already mentioned in the Introduction, the FS’s computed for the cubic phase at compositions outside the range of stability of the phase (Figs. 1, 3, and 4) are nevertheless relevant for experiments, especially where one probes the momentum density of the electron gas. We elaborate on this point now.

In a positron-annihilation or high-resolution Compton scattering experiment,^{18,19,29} the underlying spectral function involved is the 3D momentum density $\rho(\mathbf{p})$ of the ground state. The FS signatures, which are scattered throughout the momentum space in $\rho(\mathbf{p})$ can, in principle,³⁰ be enhanced by folding $\rho(\mathbf{p})$ into the first BZ to obtain a direct map of the occupied states,³¹ i.e.,

$$n(\mathbf{k}) = \sum_{\mathbf{G}} \rho(\mathbf{k} + \mathbf{G}), \quad (3)$$

where $n(\mathbf{k})$ is the occupation number for the Bloch state \mathbf{k} , and the summation extends over the set $\{\mathbf{G}\}$ of reciprocal lattice vectors. The FS may then be defined as the surface of maximum gradient of $n(\mathbf{k})$.³² As already emphasized, the orthorhombic as well as the monoclinic phase of $\text{Ba}_{1-x}\text{K}_x\text{BiO}_3$ is derived via relatively small tilting and breathing distortions of BiO_6 octahedra. It will be sensible, therefore, to obtain $n(\mathbf{k})$ from measured momentum densities by using vectors of the sc lattice in Eq. 3 at all compositions of $\text{Ba}_{1-x}\text{K}_x\text{BiO}_3$. The evolution of the FS of $\text{Ba}_{1-x}\text{K}_x\text{BiO}_3$ with doping depicted in Figs. 1–4 should in this way be essentially verifiable experimentally despite the intervention of phase transitions. As the cubic symmetry is broken with doping and various gaps open up, the momentum density will be smeared over a range of approximately E_{gap}/v_F , where E_{gap} is the energy gap and v_F is the Fermi velocity of the associated metallic state;³³ this should, however, only produce relatively small modulations of $n(\mathbf{k})$

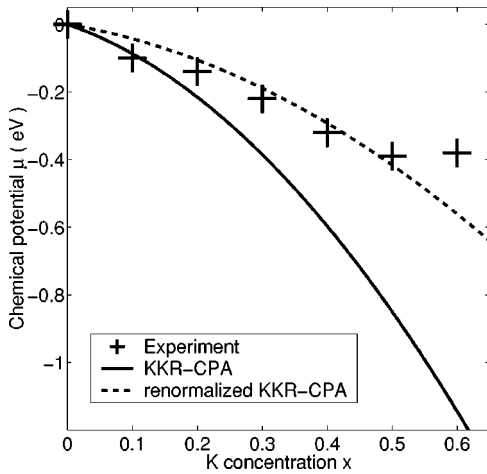


FIG. 7. Chemical potential $\mu(x)$ as a function of K concentration x obtained from photoemission experiments of Ref. 34 is seen to be in reasonable accord with KKR-CPA predictions renormalized by 0.49 (dashed). Solid curve is the theoretical result based on Eq. (2).

based on the sc structure. In this vein, disorder effects in general yield a momentum smearing, $\Delta k = \gamma/v_F$ in terms of the disorder-induced width (in energy) γ , although the value of γ in $\text{Ba}_{1-x}\text{K}_x\text{BiO}_3$ is negligibly small at the Fermi energy.

An interesting recent experimental result concerns the shift in chemical potential $\mu(x)$ as a function of doping obtained by Kobayashi *et al.*³⁴ via x-ray photoemission spectroscopy core level measurements in $\text{Ba}_{1-x}\text{K}_x\text{BiO}_3$. Figure 7 shows that KKR-CPA predictions can be brought into line with the measurements provided the theoretical values are scaled down by a factor of 0.49 (dashed curve), indicating that the dispersion of the quasiparticles near the Fermi energy may be given incorrectly in the underlying band structure. [The solid curve is the fit to the KKR-CPA values given by Eq. (2)]. This is not surprising since it is well known that the excitation energies in general do not correspond to the eigenvalues of the Kohn-Sham equation.³⁵ Notably, Ref. 34 reports absence of any abrupt changes in the chemical potential through the orthorhombic and monoclinic phase transitions; however, any such jumps in $\mu(x)$ are expected to be small in light of the discussion of preceding sections, and lie presumably below the experimental resolution. Also, core level shifts could be affected by crystal defects which may explain part of the discrepancy between theory and experiment.³⁶

IV. SUMMARY AND CONCLUSIONS

We have obtained 3D Fermi surfaces in cubic $\text{Ba}_{1-x}\text{K}_x\text{BiO}_3$ over the entire composition range; representa-

tive results for $x = 0.67, 0.4, 0.13,$ and 0.0 are presented and discussed. The computations employ the self-consistent KKR-CPA approach for treating the effects of Ba/K substitution within the framework of the local density approximation, but are parameter free otherwise. An examination of changes in the topology of the FS gives insight into transformations of the cubic phase into noncubic structures as a function of K doping. Highlights of our specific conclusions are as follows.

(1) The cubic-orthorhombic transition around $x = 0.37$ is suggested to be a Hume-Rothery type instability when the FS makes contact with the BZ of the associated fcc lattice along the (111) directions. The orthorhombic-monoclinic transition around $x = 0.13$ is interpreted within a Van Hove–Jahn-Teller scenario as the FS makes contact with the X symmetry point of the BZ.

(2) A parametrization scheme that allows an accurate determination of the 3D Fermi surface in cubic $\text{Ba}_{1-x}\text{K}_x\text{BiO}_3$ for an arbitrary doping level via a straightforward use of Eqs. (1) and (2) is developed. This scheme would be useful more generally for applications requiring FS integrals (e.g., response function computations) in $\text{Ba}_{1-x}\text{K}_x\text{BiO}_3$.

(3) We remark on the puzzling differences between the phase diagrams of $\text{Ba}_{1-x}\text{K}_x\text{BiO}_3$ and $\text{BaPb}_x\text{Bi}_{1-x}\text{O}_3$ by comparing the KKR-CPA electronic structures of $\text{Ba}_{1-x}\text{K}_x\text{BiO}_3$ and $\text{BaPb}_x\text{Bi}_{1-x}\text{O}_3$ and of the end compounds BaBiO_3 , KBiO_3 , and BaPbO_3 . The Van Hove singularity in the highest occupied Bi-O band which is virtually unaffected by Ba/K substitution is found to be smeared strongly by Pb/Bi substitution, a fact which may be relevant in this connection.

(4) Concerning experimental aspects, we show that the FS's in the cubic phase will be useful in analyzing high-resolution Compton scattering and positron-annihilation measurements on the one hand, and in verifying the present theoretical predictions on the other, suggesting the value of further experimental work along these lines. We comment also on the band renormalization in $\text{Ba}_{1-x}\text{K}_x\text{BiO}_3$ implied in the light of some recent photoemission experiments.

ACKNOWLEDGMENTS

This work was supported by the U.S. Department of Energy under Contract No. W-31-109-ENG-38 and the Academy of Finland, and benefited from the allocation of time at the NERSC, the Northeastern University Advanced Scientific Computation Center (NU-ASCC), the Center for Scientific Computing, Helsinki, and the Institute of Advanced Computing, Tampere, and from a travel grant from NATO.

¹L.F. Mattheis, E.M. Gyorgy, and D.W. Johnson, Phys. Rev. B **37**, 3745 (1988).

²R.J. Cava, B. Batlogg, J.J. Krajewski, R. Farrow, L.W. Rupp, Jr., A.E. White, K. Short, W.F. Peck, and T. Kometani, Nature (London) **332**, 814 (1988).

³Q. Huang, J.F. Zasadzinski, N. Tralshawala, K.E. Gray, D.G. Hinks, J.L. Peng, and R.L. Greene, Nature (London) **347**, 393 (1990).

⁴A.I. Liechtenstein, I.I. Mazin, C.O. Rodriguez, O. Jepsen, O.K. Andersen, and M. Methfessel, Phys. Rev. B **44**, 5388 (1991).

- ⁵V. Merregalli and S.Y. Savrasov, Phys. Rev. B **57**, 14 453 (1998).
- ⁶N. Hamada, S. Massidda, A. Freeman, and J. Redinger, Phys. Rev. B **40**, 4442 (1989).
- ⁷M. Peter, M. Weger, and L.P. Pitaevskii, Ann. Phys. (Leipzig) **7**, 174 (1998).
- ⁸M. Dayan, J. Supercond. **11** 417 (1998).
- ⁹P. Kumar, D. Hall, and R.G. Goodrich, Phys. Rev. Lett. **82**, 4532 (1999); see also, B. F. Woodfield, D. A. Wright, R. A. Fisher, and N. E. Phillips, Phys. Rev. Lett. **83**, 4622 (1999).
- ¹⁰B.A. Baumert, J. Supercond. **8**, 175 (1995).
- ¹¹S. Pei, J.D. Jorgensen, B. Dabrowski, D.G. Hinks, D.R. Richards, A.W. Mitchell, J.M. Newsam, S.K. Sinha, D. Vaknin, and A.J. Jacobson, Phys. Rev. B **41**, 4126 (1990).
- ¹²L.F. Mattheis and D. Hamann, Phys. Rev. B **28**, 4227 (1983).
- ¹³L.F. Mattheis and D. Hamann, Phys. Rev. Lett. **60**, 2681 (1988).
- ¹⁴A. Bansil and S. Kaprzyk, Phys. Rev. B **43**, 10 335 (1991).
- ¹⁵S. Kaprzyk and A. Bansil, Phys. Rev. B **42**, 7358 (1990).
- ¹⁶A. Bansil, S. Kaprzyk, P. E. Mijnaerends, and J. Tobola, Phys. Rev. B. **60**, 13 396 (1999).
- ¹⁷U. von Barth and L. Hedin, J. Phys. C **5**, 1629 (1972).
- ¹⁸A. Bansil, Z. Naturforsch., A: Phys. Sci. **48**, 165 (1993).
- ¹⁹A. Bansil, in *Positron Annihilation*, edited by P.G. Coleman, S.G. Sharma, and L.M. Diana, (North-Holland, Amsterdam, 1982), p. 273.
- ²⁰D.E. Cox and A.W. Sleight, Solid State Commun. **19**, 969 (1976); Acta Crystallogr., Sect. B: Struct. Sci. **B35**, 1 (1979).
- ²¹M. Weger, B. Barbiellini, and M. Peter, Z. Phys. B **94**, 387 (1994).
- ²²W. Hume-Rothery and G.V. Raynor, *Structures of Metals and Alloys*, 4th ed. (Inst. of Metals, London, 1962).
- ²³A.P. Blandin, *Phase Stability in Metals and Alloys*, edited by P.S. Rudman, J. Stringer, and R.I. Jaffee (McGraw-Hill, New York, 1967), p. 115; J. Hafner, *From Hamiltonians to Phase Diagrams* (Springer, Berlin, 1987).
- ²⁴M. Hansen, *Constitution of Binary Alloys* (McGraw-Hill, New York, 1958).
- ²⁵R.S. Markiewicz, Physica C **200**, 65 (1992).
- ²⁶T.M. Rice, and G.K. Scott, Phys. Rev. Lett. **35**, 120 (1975).
- ²⁷R.S. Markiewicz, J. Phys. Chem. Solids **58**, 1179 (1997).
- ²⁸W.D. Mosley, J.W. Dykes, R.N. Shelton, P.A. Sterne, and R.H. Howell, Phys. Rev. Lett. **73**, 1271 (1994).
- ²⁹P.E. Mijnaerends and A. Bansil, in *Positron Spectroscopy of Solids*, Proceedings of the International School of Physics ‘‘Enrico Fermi,’’ Course CXXV, 1993, edited by A. Dupasquier and A.P. Mills, Jr. (IOS Press, Amsterdam, 1995), pp. 25–74.
- ³⁰We set aside here issues of resolution and statistics, and other practical matters tied to the fact that Compton measures a 2D integral and the positron annihilation a 1D or a 2D integral of $\rho(\mathbf{p})$ and involves complications introduced by the positron wave function.
- ³¹D.G. Lock, V.H.C. Crisp, and R.N. West, J. Phys. F: Met. Phys. **3**, 561 (1973).
- ³²In a correlated system, the definition of the FS is more subtle. For instance, Luttinger’s theorem defines the FS as the surface in \mathbf{k} space at which the real part of the $G(\mathbf{k}, E = E_F)$ changes sign; see J. Negele and H. Orland, *Quantum Theory of Many-Particle Systems*, (Addison-Wesley, Redwood City, CA, 1988).
- ³³J. Friedel and M. Peter, Europhys. Lett. **8**, 79 (1989).
- ³⁴K. Kobayashi, T. Mizokawa, A. Ino, J. Matsuno, A. Fujimori, H. Samata, A. Mishiro, Y. Nagata, and F.M.F. de Groot, Phys. Rev. B **59**, 15 100 (1999).
- ³⁵R.O. Jones and O. Gunnarsson, Rev. Mod. Phys. **61**, 689 (1989).
- ³⁶H. Nylén, A. Beutler, A.A. Zakharov, M. Leandersson, M. Qvarford, I. Lindau, M.B. Tselin, L.L. Lev, M.N. Mikheeva, S.N. Barilo, and S.V. Shiryayev, Phys. Rev. B **58**, 12 836 (1998).